


 Cite this: *New J. Chem.*, 2018, 42, 15871

Co-N-C catalysts synthesized by pyrolysis of Co-based deep eutectic solvents for aerobic oxidation of alcohols†

 Xin Zhao,^a Yan Zhou,^a Ai-Ling Jin,^a Kuan Huang,^b Fujian Liu^{*c} and Duan-Jian Tao^{id}^{*a}

The selective oxidation of alcohols to the corresponding aldehydes and ketones is of great importance in the academic and industrial fields. A series of excellent nanostructured catalysts comprising cobalt nanoparticles supported on nitrogen-doped carbon (Co-N-C) were thus prepared by pyrolysis of a deep eutectic solvent $\text{Co}(\text{NO}_3)_2 \cdot 6\text{H}_2\text{O}/[\text{Bmim}]\text{Br}$ supported on commercial carbon. The catalytic activity of the Co-N-C materials was studied in the selective aerobic oxidation of alcohols with molecular oxygen under base-free conditions. The results indicated that the optimized Co-N-C/700 catalyst exhibited excellent catalytic performance in the selective oxidation of both aryl and alkyl alcohols, giving their corresponding aldehydes and ketones in good to excellent yields. Furthermore, the combination of the catalytic results of the control group and the different characterization methods showed that such high catalytic activity is due to the synergistic interaction between the nitrogen-doped carbon support and Co-N species in Co-N-C/700. In addition, the magnetically recoverable Co-N-C catalyst could be easily separated from the reaction system by using an external magnetic field and reused at least five times without an obvious decrease in the catalytic efficiency.

 Received 10th July 2018,
 Accepted 20th August 2018

DOI: 10.1039/c8nj03446j

rsc.li/njc

Introduction

The selective oxidation of alcohols to the corresponding aldehydes/ketones is an important reaction in the chemical industry, to build up complex molecules from readily available substrates.^{1,2} Recently, a large number of metal-based heterogeneous catalysts have been developed to promote the chemical transformation from benzyl alcohol to benzaldehyde, since heterogeneous catalysts are preferred industrially due to their low cost and ease of separation and reuse. For example, Beller *et al.* reported that $\text{Co}_3\text{O}_4\text{-N@C}$ was a promising catalyst in the oxidation of alcohols, in which the cross and self-esterification of alcohols to esters proceeds in good to excellent yields.³ Li *et al.* prepared MOF-derived Co catalysts, which exhibited excellent catalytic

performance in the selective oxidation of benzyl alcohol.⁴ Also, many other supported cobalt-based catalysts such as N-doped cobalt-graphene composites, Co-N-C immobilized on CNTs, and $\text{Co}_3\text{O}_4/\text{AC}$ (activated carbon) were found to have good catalytic activities.^{5–8} Nonetheless, the catalytic performance is still not satisfactory because an additional base additive was usually required, peroxides were employed as terminal oxidants, and furthermore, metal nanoparticles are prone to leaching or/and aggregation, leading to the deterioration of the catalytic activity in some cases.^{9–11} Given the demand for a sustainable and environmentally friendly reaction process with zero additives and by-products, the construction of an environmentally benign base-free aerobic oxidation system is highly desirable. In addition, further promoting the catalytic activity of transition-metal nanoparticle-based catalysts should be the most direct approach to meet the requirements for green chemistry.¹² Therefore, it is essential to develop a novel synthesis strategy for metal nanoparticle catalysts for efficient heterogeneous catalysis with high recyclability.

Ionic liquids (ILs) typically serving as excellent solvents and functional materials have been attracting much attention in diverse areas such as organocatalysis, gas separation, biomass degradation and electrolytes in batteries and fuel cells.^{13–17} Deep eutectic solvents (DESS), representing a new class of IL analogues, have attracted great interest because of their diverse

^a College of Chemistry and Chemical Engineering, Institute of Advanced Materials, Jiangxi Normal University, Nanchang, Jiangxi 330022, China. E-mail: djtao@jxnu.edu.cn

^b Key Laboratory of Poyang Lake Environment and Resource Utilization of Ministry of Education, School of Resources Environmental and Chemical Engineering, Nanchang University, Nanchang, Jiangxi 330031, China

^c National Engineering Research Center of Chemical Fertilizer Catalyst (NERC-CFC), School of Chemical Engineering, Fuzhou University, Fuzhou, Fujian 350002, China. E-mail: liufujian1982@163.com

† Electronic supplementary information (ESI) available: Additional characterization and reaction results. See DOI: 10.1039/c8nj03446j

and tunable compositions, structures, and properties, as well as various potential applications and they can be considered as promising alternatives to ILs.¹⁸ They are usually obtained by the complexation of a hydrogen bond receptor (HBR) with a hydrogen bond donor (HBD).¹⁹ Notably, the metal-containing DES is a novel representation with abundant carbon and nitrogen ligands, and high metal ion contents. Benefiting from the strong hydrogen bonding between the HBR and HBD, the metal-containing DES is expected to be a good candidate as a precursor template or sacrificial agent to design various porous nanostructured metal and nitrogen bi-modified carbon materials (M-N-C).

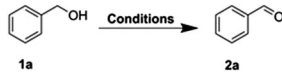
Based on the above considerations and inspired by the strategy of the construction of carbon supported metal nanocomposites *via* the pyrolysis of metal-coordinated copolymers,^{20–22} we designed and prepared several metal-containing DESs and fabricated the corresponding M-N-C materials, which are expected to have the following advantages. First, compared with other traditional metal solutions, the metals in the DESs are uniformly dispersed and have strong hydrogen bonding with the ligand, affording stable microenvironments of encapsulated metals. Second, the rich nitrogen species could partially dope into the as-prepared M-N-C materials during pyrolysis, and the evaporation of non-metallic elements would contribute to a small portion of the pore structure in such materials. All these features make the metal-containing DES derived M-N-C an exciting material *via* a novel pyrolysis method.

Herein, we designed and prepared a series of highly efficient DES-derived cobalt catalysts (nitrogen-doped carbon embedded cobalt nanoparticles, Co-N-C). They were prepared simply by pyrolysis of the precursor commercial carbon impregnated DES consisting of 1-butyl-3-methylimidazolium bromide and cobalt salts. Combining the abundant exposed Co-N active sites, fast diffusion of reactants/products, and improved structural stability offered by the sacrificed DES retained rich pores and given the relatively high surface area, a highly enhanced catalytic activity was obtained as well as a high durability in the selective aerobic oxidative reaction of benzyl alcohols. Furthermore, the prepared Co-N-C catalytic system features a broad substrate scope for aromatic and aliphatic alcohols, giving their corresponding aldehydes in good to excellent yields. These catalysts could also be quickly recovered by magnetic separation and reused without losing activity. It is believed that this pyrolyzing strategy of the Co-containing DES can be expanded to construct other catalytically active M-N-C catalysts for a wide range of applications.

Results and discussion

Alcohol oxidation reactions were performed under base-free conditions using an atmospheric pressure of oxygen as the terminal oxidant. The experimental results are summarized in Table 1. The Co-N-C materials were assessed as catalysts for the aerobic oxidation of benzyl alcohol in toluene at 100 °C. It can be seen that the Co-N-C materials displayed various catalytic activities in the oxidation of benzyl alcohol (Table 1, entries 1–4), in which Co-N-C/700

Table 1 Optimization of reaction conditions for the oxidation of benzyl alcohol to benzaldehyde

				
Entry	Catalyst	Solvent	Conv. (%)	Yield (%)
1	Co-N-C/600	Toluene	57	56
2	Co-N-C/700	Toluene	92	92
3	Co-N-C/800	Toluene	74	72
4	Co-N-C/900	Toluene	67	66
5	Co-N-C/700	Octane	99	15
6	Co-N-C/700	DMF	52	51
7	Co-N-C/700	DMSO	50	50
8	Co-N-C/700	Hexanol	38	38
9 ^a	Co-N-C/700	Toluene	57	57
10 ^b	Co-N-C/700	Toluene	26	26
11 ^c	Co-N-C/700	Toluene	56	55
12 ^d	Co-N-C/700	Toluene	10	7

Reaction conditions: **1a** (1.0 mmol), catalyst (10 mol% Co), solvent (5 mL), O₂ balloon, 100 °C and 36 h. The main primary by-product for the selective oxidation of benzyl alcohol is benzoic acid. ^a 12 h. ^b 50 °C. ^c Catalyst (5 mol% Co). ^d Filled with N₂ balloon.

was the most active catalyst, obtaining a 92% conversion of benzyl alcohol and 92% yield of benzaldehyde. After screening the reaction parameters, the optimized conditions can be set as follows: 10 mol% Co-N-C/700, toluene as the solvent, O₂ as the oxidant, temperature of 100 °C and reaction time of 36 h (Table 1, entries 5–12).

Inspired by these intriguing results, we further prepared a series of C-containing, N-containing, and Co-based materials and employed them as reference catalysts to support the outstanding catalytic properties of the Co-N-C/700 composite in aerobic oxidation. The results are listed in Table 2. It is indicated that the oxidation reaction hardly occurred without any catalysts, while Vulcan XC72R carbon and [Bmim]Br were inactive for the oxidation of benzyl alcohol (Table 2, entries 1–3). The catalytic Co salts Co(NO₃)₂ and Co₃O₄ also gave low benzaldehyde

Table 2 Selective oxidation of benzyl alcohol catalyzed by various catalysts

Entry	Catalyst	Conv. (%)	Yield (%)
1	—	<1	<1
2	Vulcan XC72R	<1	<1
3	[Bmim]Br	18	14
4	Co(NO ₃) ₂	98	33
5	Co ₃ O ₄	47	47
6	Co-C/700	<1	<1
7	N-C/700	<1	<1
8	Co-N/700	9	9
9 ^a	Co-C	99	28
10 ^b	Co-C (NaBH ₄)	<1	<1
11 ^c	Co-N-C/700	90	89
12 ^d	Co-N-C/700	87	86
13 ^e	Co-N-C/700	61	61
14 ^f	Co-N-C/700	73	71

Reaction conditions: **1a** (1.0 mmol), catalyst (10 mol% Co), toluene (5 mL), O₂ balloon, 100 °C and 36 h. The main primary by-product for the selective oxidation of benzyl alcohol is benzoic acid. ^a Co-C was prepared by an impregnation method. ^b Reduction with NaBH₄. ^c Co(OAc)₂·4H₂O. ^d CoCl₂·6H₂O. ^e [Bpy]Br. ^f TBAB.

yields of 33% and 47%, respectively (Table 2, entries 4 and 5). Notably, the Co-C/700 and N-C/700 catalysts exhibited very poor catalytic performance under identical conditions (Table 2, entries 6 and 7), showing the importance of N-doping and metallic Co in the composite for the oxidation reaction. Meanwhile, Co-N/700 had low activity in the oxidation of benzyl alcohol because of the absence of Vulcan XC72R carbon as a support in the pyrolysis process (Table 2, entry 8). Co-C prepared by the impregnation method exhibited good conversion but poor selectivity compared to $\text{Co}(\text{NO}_3)_2$, where Co-C lost the catalytic activity after the reduction with NaBH_4 (Table 2, entries 9 and 10). Furthermore, various Co and N-containing precursors using other cobalt salts and N-doping sources were studied for the preparation of Co-N-C/700 catalysts, in which moderate to good yields of benzaldehyde could be achieved (Table 2, entries 11–13). Thus, these control experiments suggested that the synergic interaction between Co species and N-doped carbon played a significant role in determining the excellent performance of Co-N-C/700 in the oxidation of benzyl alcohol.

In order to clarify the remarkable catalysis behavior of Co-N-C/700 in the aerobic oxidation of alcohols, a series of characterization techniques were carried out to get the characteristics of the catalysts. As shown in Table 3, the Co content of the composites was 8–11 wt%, and the nitrogen content decreased from 4.5% to 1.4% when the pyrolysis temperature increased from 600 °C to 900 °C. Compared with other Co-based materials, the Co-N-C/700 composite had a higher surface area, a higher pore volume, and a larger pore size. This shows that a relatively high temperature would probably cause the decomposition of the mesoporous structure and leads to the lower surface area.²³ The large surface area and pore size of the Co-N-C/700 composite was beneficial to the Co metal dispersions and could promote the mass transfer process of reactants and thus resulted in a good reactivity, which could be observed from the SEM and XRD results.

Fig. 1 shows the XRD patterns of the Co-N-C composites. A broad peak at 25° could be assigned to the (002) interlayer of graphite-type carbon sheets. For Co-N-C/600, no diffraction peak of cobalt was found from the XRD patterns, showing that the cobalt species were amorphous at 600 °C. For the other three Co-N-C composites, the peaks at 44.1°, 51.4°, and 75.9° could be indexed to the (111), (200), and (220) crystalline planes of the face-centered cubic structure of metallic cobalt (PDF#15-0806), respectively, indicating the existence of metallic Co.^{17,22–24} The metallic Co might be formed by reducing the Co-based precursors with carbon species at high temperatures. Moreover, it can be seen that with an increase of pyrolyzing

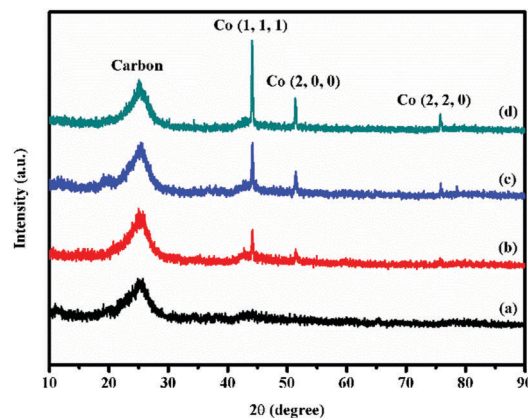


Fig. 1 XRD patterns of (a) Co-N-C/600, (b) Co-N-C/700, (c) Co-N-C/800 and (d) Co-N-C/900.

temperature, more intense diffraction peaks of the cobalt species were detected, implying the presence of a high proportion of reduced Co at high temperatures.

Raman spectroscopy is commonly used to measure carbon-based catalysts. The D band at 1325 cm^{-1} and the G band at 1590 cm^{-1} of the Co-N-C composites were detected in the Raman spectra (Fig. 2). It is known that the D band is related to the disordered structure of materials, including the defects in the graphene lattice and amorphous carbon. The G band corresponds to the vibration peak of the ideal sp^2 hybridized carbon atom, showing the integrity of the graphene layer. Then, the intensity ratio of the D band to the G band, termed I_D/I_G , is used to estimate the defects of carbon-based nanostructures.^{25–27} It is shown that upon increasing the pyrolyzing temperature, the I_D/I_G ratio decreased slightly from 1.36 at 600 °C to 1.09 at 800 °C, indicating the increased crystallization degree of graphitic carbon, which was in good agreement with the results obtained from the XRD patterns.

The morphologies and metal dispersions of the Co-N-C composites were investigated using SEM and HRTEM. As shown in Fig. 3, typical nanosheet structures were observed in the Co-N-C materials. For the Co-N-C/700 catalyst, from the scanning electron

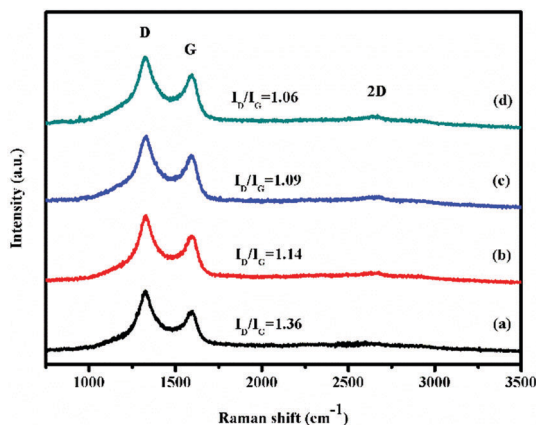


Fig. 2 Raman spectra of (a) Co-N-C/600, (b) Co-N-C/700, (c) Co-N-C/800 and (d) Co-N-C/900.

Table 3 Properties of Co-N-C catalysts

Sample	S_{BET} ($\text{m}^2 \text{g}^{-1}$)	Pore volume ($\text{cm}^3 \text{g}^{-1}$)	Pore size (\AA)	Content (wt%)			
				C ^a	N ^a	H ^a	Co ^b
Co-N-C/600	96	0.03	2.4	75.6	4.5	0.8	8.1
Co-N-C/700	216	0.07	3.3	76.3	3.3	0.9	9.6
Co-N-C/800	165	0.03	2.0	84.2	1.5	0.6	10.5
Co-N-C/900	177	0.04	1.8	86.3	1.4	0.6	11.6

^a Measured by elemental analysis. ^b Measured by ICP-OES.

microscopy image, it can be seen that the material is suitably uniform in size and homogeneous in morphology. At elevated pyrolyzing temperatures (800 and 900 °C), the size of the observed nanosheets decreased and aggregation gave rise to low BET surface areas, which was in accordance with the results obtained from nitrogen adsorption/desorption analysis. In addition, it can be seen from Fig. 4 that the Co particles were well-dispersed on the N-doped carbon in Co-N-C/700 with a uniform particle size. The (111) and (200) *d*-spacing of metallic Co nanoparticles could be clearly measured as 0.208 nm and 0.177 nm,²⁸ which is in good agreement with the XRD measurements. For comparison, the HRTEM image indicated that the Co nanoparticles in the Co-C/700 material were seriously aggregated with much bigger clusters (Fig. S3, ESI†). This finding demonstrated that the N-containing

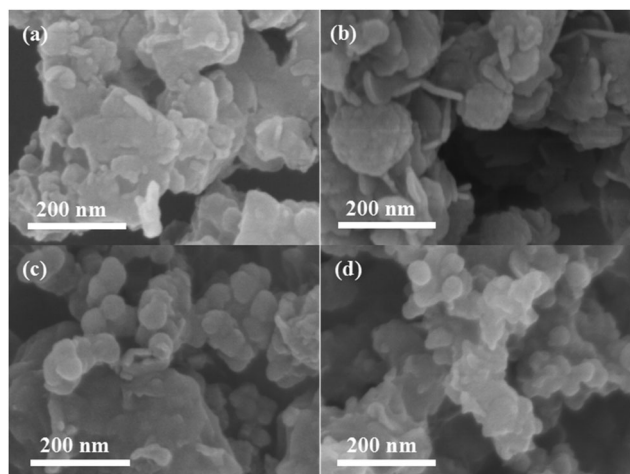


Fig. 3 SEM images of (a) Co-N-C/600, (b) Co-N-C/700, (c) Co-N-C/800 and (d) Co-N-C/900.

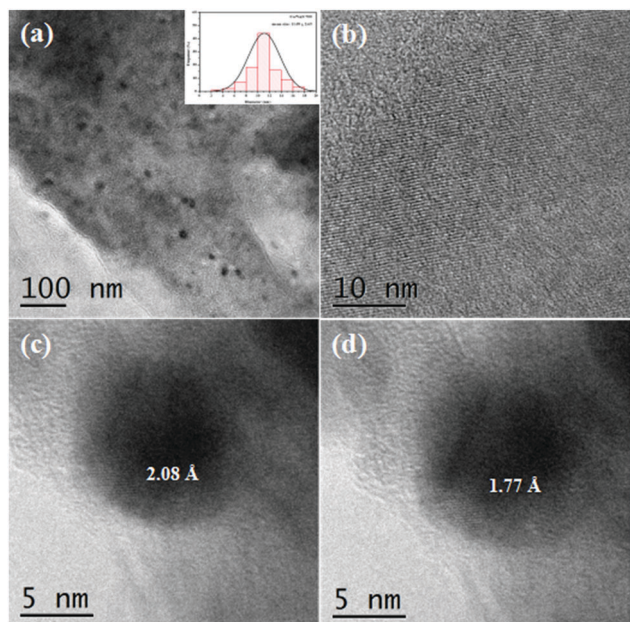


Fig. 4 TEM images and the size distribution of Co particles in Co-N-C/700.

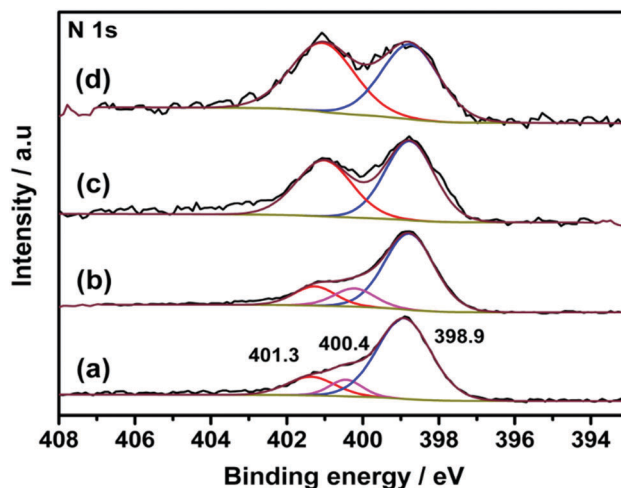


Fig. 5 N 1s spectra for (a) Co-N-C/600, (b) Co-N-C/700, (c) Co-N-C/800 and (d) Co-N-C/900.

precursor [Bmim]Br plays an important role in highly dispersing the Co particles on graphitized carbon and reducing the particle size of Co particles.

In order to gain further insight into the valence states of Co, N, and O, XP spectra of N 1s and Co 2p of the Co-N-C catalysts are shown in Fig. 5 and 6. Regarding the N 1s XP spectra (Fig. 5), three distinct peaks can be observed for the Co-N-C materials with electron binding energies of pyridinic N (398.9 eV), pyrrolic N (400.4 eV), and graphitic N (401.3 eV).^{29–31} It was found that the percentage of pyridinic N decreased as the pyrolysis temperature increased, due to the graphitization of the precursor DES and commercial carbon. The relative content of pyridinic N in Co-N-C/700 was higher than that in the other two Co-N-C/800 and Co-N-C/900 samples. Previous studies indicated that pyridine-type nitrogen can stabilize metal particles and provide the required Lewis basicity to improve the catalytic activity for the oxidation of hydrocarbons and alcohols.^{32–36} Thus, the Co-N-C/700 catalyst

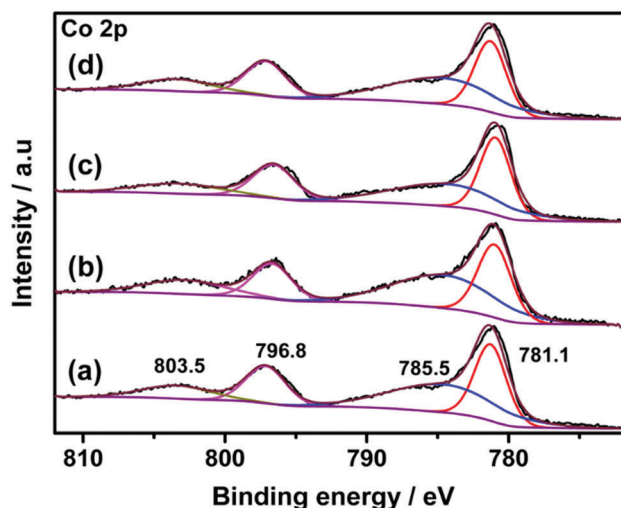


Fig. 6 Co 2p spectra for (a) Co-N-C/600, (b) Co-N-C/700, (c) Co-N-C/800 and (d) Co-N-C/900.

showed good catalytic performance in the aerobic oxidation of benzyl alcohol.

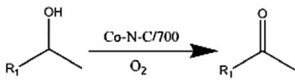
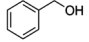
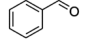
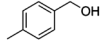
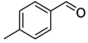
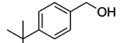
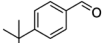
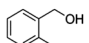
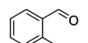
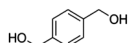
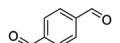
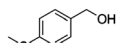
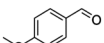
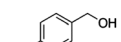
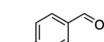
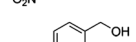
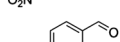
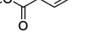
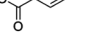
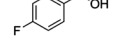
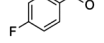
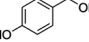
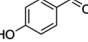
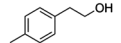
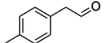
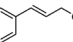
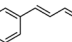
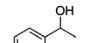
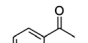
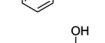
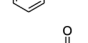
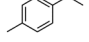
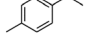
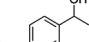
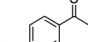
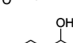

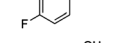
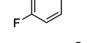
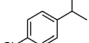
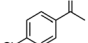
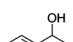
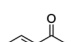
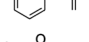
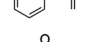
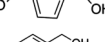
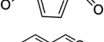
Moreover, the O 1s spectrum was deconvoluted into a peak at 532.1 eV (Fig. S4, ESI[†]). According to the literature,^{37–40} it could belong to both adsorbed oxygen and a little amount of C–O group in the graphitic carbon, indicating the absence of any Co–O species in the Co–N–C catalysts. In the cobalt region, the binding energies at 781.1 eV and 796.8 eV were assigned to Co 2p_{3/2} and Co 2p_{1/2} of Co–N, respectively.^{29,41,42} The broad peaks at 785.5 eV and 803.5 eV can be attributed to the shake-up satellite peaks of Co–N. However, no Co⁰ species was detected by XPS, implying that all the Co⁰ nanoparticles were probably shielded by the thick graphitic layers encapsulating the Co⁰ particles so that they could not be probed by the surface-sensitive XPS.⁴³ Then, we conducted XPS measurement for the Co–N–C/700 catalyst using Ar⁺ ion-beam etching. The results showed that the Co 2p_{3/2} peak of metallic Co was successfully observed and appeared at 778.9 eV^{18,44,45} (Fig. S5, ESI[†]). But, the peaks at 782.5 eV and 794.5 eV were attributed to Co³⁺ because of the oxidation of metallic Co to Co₃O₄ during the etching procedure.

Therefore, the XPS characterization results demonstrated that compared with the Co⁰ nanoparticles, the Co–N species in Co–N–C/700 was believed to be the active site for the highly efficient aerobic oxidation of alcohols. The encapsulated Co⁰ nanoparticles in the N-doped carbon nanosheets struggle to participate in the aerobic oxidation reaction. Furthermore, the high catalytic activity over Co–N–C/700 was also attributed to the contribution of its highest BET surface area (Table 3). The large surface area is favorable for exposure of the catalytically active sites to reactants and thereby leads to excellent catalytic performance.

In order to investigate the applicability of the Co–N–C/700 catalyst, the selective oxidation of various alcohols was further studied with molecular oxygen under base-free conditions (Table 4). It can be seen that various benzyl alcohols bearing electron-donating and electron-withdrawing groups could provide the corresponding substituted benzaldehydes in good to excellent yields under identical conditions (Table 4, entries 1–11). Moreover, by prolonging the reaction time to 48 h, cinnamyl alcohol was oxidized to cinnamyl aldehyde with a yield of 76% (Table 4, entry 12). Also, acetophenone was obtained in 91% yield *via* the oxidation of 1-phenylethanol (Table 4, entry 13). Four *p*-substituted phenylethanols further afforded the corresponding substituted ketones in 70–84% yields (Table 4, entries 14–17). The oxidations of α -vinylbenzyl alcohol and 5-hydroxymethylfurfural to α -vinylbenzyl aldehyde and 2,5-furandicarbaldehyde were observed in 77% and 68% yields, respectively (Table 4, entries 18 and 19). 3-Pyridylmethanol gave a 95% yield of 3-pyridinecarboxaldehyde (Table 4, entry 20). However, it was indicated that the oxidation of primary alcohols was difficult to perform and gave the corresponding aldehydes with frustrated yields, although the catalyst amounts of Co–N–C/700 increased (Table 4, entries 21–23).

Finally, the reusability of the Co–N–C/700 catalyst in the aerobic oxidation of benzyl alcohol was explored. The catalyst

Table 4 Selective oxidation of various alcohols catalyzed by Co–N–C/700

				
Entry	Substrate	Product	Conv. (%) ^a	Yield (%) ^a
1			92	92
2			91	91
3			83	83
4			70	70
5			> 99	> 99
6			> 99	> 99
7			98	98
8			81	81
9			72	72
10			88	88
11			80	80
12 ^b			76	76
13 ^b			91	91
14 ^b			83	83
15 ^b			84	84
16 ^b			74	74
17 ^b			70	70
18			77	77
19			68	68
20			95	95
21 ^c			20	20
22 ^c			20	20
23 ^c			21	21

Reaction conditions: Alcohol (1.0 mmol), catalyst (10 mol% Co), toluene (5 mL), O₂ balloon, 100 °C and 36 h. ^a Conversion and yield were determined by GC-MS. ^b 48 h. ^c Catalyst (20 mol% Co).

could be separated from the reaction mixture using an external magnet after the reaction. The recycling experiment result is

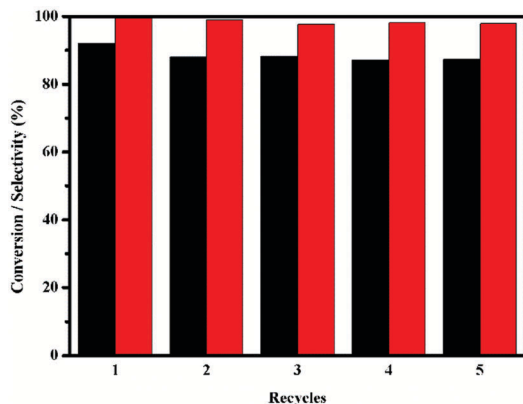


Fig. 7 Recovery and reuse of the Co-N-C/700 catalyst.

shown in Fig. 7. It is clear that no obvious decrease in both the conversion of benzyl alcohol and selectivity of benzaldehyde was observed during five successive recycles. No significant change in the morphology and structure of the Co-based species was observed in the SEM image and XRD pattern of the recycled Co-N-C/700 catalyst (Fig. S6 and S7, ESI†). Compared with the fresh catalyst, the Raman spectral characteristic bands also appeared in the reused Co-N-C/700 catalyst (Fig. S8, ESI†). This further demonstrated that Co-N-C/700 could be stable enough to be used in the aerobic oxidation for several runs.

Conclusions

In summary, we have reported the employment of Co-N-C composites as efficient heterogeneous catalysts for the direct and selective oxidation of alcohols into the corresponding aldehydes and ketones, with molecular oxygen as a clean oxidant under base-free conditions. The results of the catalytic studies of the control group and several characterization investigations demonstrated that such high catalytic efficiency resulted from the synergistic interaction between the nitrogen-doped carbon support and Co-N species in the Co-N-C/700 catalyst. We believe that the utilization of a deep eutectic solvent as the precursor provides a novel strategy to prepare highly efficient non-precious metal-based catalysts and also shows great potential for the synthesis of carbonyl compounds through selective alcohol oxidation.

Experimental

Materials

VULCAN XC72R with Code XVC72R and CAS No. 1333-86-4 was obtained from Cabot Corporation Prod. 1-Butyl-3-methylimidazolium bromide ([Bmim]Br, 99%), butylpyridinium bromide ([Bpy]Br, 99%), and tetrabutylammonium bromide (TBAB, 99%) were purchased from the Centre of Green Chemistry and Catalysis, LICP, CAS. $\text{Co}(\text{NO}_3)_2 \cdot 6\text{H}_2\text{O}$ (99%), benzyl alcohol (99%), 1-phenylethanol (98%), 3-pyridinemethanol (98%), 5-hydroxymethylfurfural (97%), ethanol (99%), and methylbenzene

(99.5%) were purchased from Adamas Reagent (Shanghai). Other derivatives of benzene alcohol, phenylethanol, and primary alcohol were purchased from Energy Chemical (Shanghai). O_2 with a purity of 99.99% was commercially available. All starting materials and solvents were obtained in the highest purity grade possible and used as received.

Catalyst preparation

All of the Co-N-C catalysts were prepared through *in situ* pyrolysis methods. The catalysts were labeled as Co-N-C/*T* (where *T* is the pyrolysis temperature, which can be 600, 700, 800, or 900 °C). For example, the typical preparation procedure of Co-N-C/700 is described as follows: $\text{Co}(\text{NO}_3)_2 \cdot 6\text{H}_2\text{O}$ (1.83 g) and [Bmim]Br (4.38 g) were added to a 20 mL vial. The DES $\text{Co}(\text{NO}_3)_2 \cdot 6\text{H}_2\text{O}$ /[Bmim]Br (Fig. S1, ESI†) was thus obtained after stirring the mixture for 10 min at room temperature. Then, 2.0 g of Vulcan XC72R carbon and 40 mL of ethanol were added to the DES and the whole reaction mixture was stirred at 25 °C for 12 h. Subsequently, the ethanol solvent was removed using rotary evaporation and dried at 70 °C for 12 h. After drying, the powdered sample was placed into a quartz boat and was pyrolyzed at 700 °C for 2 h in a tubular furnace at a heating rate of 10 °C min⁻¹ under an argon gas flow. The resulting solid was cooled to room temperature to give Co-N-C/700.

The procedure for preparing Co-C/700 and Co-N/700 was the same as that for Co-N-C/700, but no [Bmim]Br and Vulcan XC72R carbon were impregnated in the mixture, respectively. The prepared material Co-N-C/700 was immersed in aqua regia to remove Co and thus obtain N-C/700.

Catalytic characterization

The cobalt contents in the samples were measured by Inductively Coupled Plasma Optical Emission Spectrometry (ICP-OES) using an Agilent 720 instrument after the sample was completely dissolved in a mixture of HNO_3/HCl (1/3 ratio). The CHN elemental contents of the catalysts were measured on an Elementar Vario El III instrument.

The BET surface area, pore volume, pore size distribution, and average pore diameter of the catalysts were characterized by using nitrogen adsorption/desorption analysis at 77 K on a Quantachrome Quadrasorb SI Instrument. Prior to the measurements, the samples were degassed at 150 °C for 4 h.

Raman spectra were obtained using a LabRAM HR spectrometer with an excitation wavelength at 632 nm with 3 cm⁻¹ spectral resolution. Powder X-ray diffraction (XRD) studies were conducted on a Rigaku RINT-2200 X-ray diffractometer with a Cu K α source at 40 kV and 20 mA.

The morphology and sizes of the samples were studied by using high-resolution transmission electron microscopy (HRTEM, JEM-2100 from JEOL). Scanning electron microscopy (SEM) images were obtained using a HITACHI SU8020 cold field-emission instrument. X-ray photoelectron spectroscopy (XPS) measurements were performed on a Thermo Scientific ESCALAB 250Xi system equipped with a hemispherical analyzer and using a monochromatic Al K α radiation source.

Catalytic reaction

The aerobic oxidation of alcohol was carried out in a 10 mL round-bottomed flask equipped with a magnetic stirrer. Typically, alcohol (1 mmol), toluene (5 mL), and Co-N-C/700 catalyst (10 mol%) were added into the reactor. The reaction mixture was stirred at 100 °C under an oxygen atmosphere for 36 h. After the reaction, the products were separated from the catalyst by using an external magnet, and then diluted with ethanol and identified by gas chromatography-mass spectrometry (GC-MS) (Thermo Trace 1300 GC-ISQ) and quantified by a GC-FID (Agilent 7890B) equipped with a capillary column HP-5 (methyl polysiloxane, 30 m × 0.32 mm × 1 µm). Trimethylbenzene was used as an internal standard to quantify the products. The detailed analysis conditions are as follows: the temperatures of the injector and detector were 280 and 250 °C, respectively. The column temperature was increased from 60 to 280 °C at 10 °C min⁻¹, holding at 280 °C for 2 min.

Recycling of catalyst

After the reaction, the catalyst was separated from the reaction mixture using an external magnet (Fig. S2, ESI[†]). Then, it was washed thoroughly with ethanol and dried at 70 °C for 12 h. After that, the catalyst was used for the next run directly.

Conflicts of interest

There are no conflicts to declare.

Acknowledgements

We thank the National Natural Science Foundation of China (No. 21566011, 31570560), the Jiangxi Province Sponsored Programs for Distinguished Young Scholars (No. 20162BCB23026), the Natural Science Foundation of Jiangxi Province (No. 20151BAB213016), and the Science & Technology Programs of Jiangxi Province Department of Education (No. GJJ160272) for financial support.

Notes and references

- B. Gutmann, D. Cantillo and C. O. Kappe, *Angew. Chem., Int. Ed.*, 2015, **54**, 6688–6728.
- N. Kan-nari, S. Okamura, S.-i. Fujita, J.-i. Ozaki and M. Arai, *Adv. Synth. Catal.*, 2010, **352**, 1476–1484.
- R. V. Jagadeesh, H. Junge, M. M. Pohl, J. Radnik, A. Bruckner and M. Beller, *J. Am. Chem. Soc.*, 2013, **135**, 10776–10782.
- C. Bai, A. Li, X. Yao, H. Liu and Y. Li, *Green Chem.*, 2016, **18**, 1061–1069.
- T. Ishida, M. Nagaoka, T. Akita and M. Haruta, *Chem. – Eur. J.*, 2008, **14**, 8456–8460.
- S. Wang, Z. Zhang and B. Liu, *ACS Sustainable Chem. Eng.*, 2015, **3**, 406–412.
- B. Liu, Z. Zhang, K. Lv, K. Deng and H. Duan, *Appl. Catal., A*, 2014, **472**, 64–71.
- Y. Qiu, C. Yang, J. Huo and Z. Liu, *J. Mol. Catal. A: Chem.*, 2016, **424**, 276–282.
- A. Saha, S. Payra and S. Banerjee, *New J. Chem.*, 2017, **41**, 13377–13381.
- A. Pourjavadi and Z. Habibi, *Appl. Organomet. Chem.*, 2017, **31**, 3783.
- P. Giorgi, N. Elizarov and S. Antonietti, *ChemCatChem*, 2017, **9**, 1830–1836.
- H. Su, K.-X. Zhang, B. Zhang, H.-H. Wang, Q.-Y. Yu, X.-H. Li, M. Antonietti and J.-S. Chen, *J. Am. Chem. Soc.*, 2017, **139**, 811–818.
- Z. Ma, J. Yu and S. Dai, *Adv. Mater.*, 2010, **22**, 261–285.
- N. V. Plechkova and K. R. Seddon, *Chem. Soc. Rev.*, 2008, **37**, 123–150.
- B. Wang, L. Qin, T. Mu, Z. Xue and G. Gao, *Chem. Rev.*, 2017, **117**, 7113–7131.
- R. D. Rogers and K. R. Seddon, *Science*, 2003, **302**, 792–793.
- V. I. Pavulescu and C. Hardacre, *Chem. Rev.*, 2017, **107**, 2615–2665.
- Q. Zhang, K. De Oliveira Vigier, S. Royer and F. Jerome, *Chem. Soc. Rev.*, 2012, **41**, 7108–7146.
- E. L. Smith, A. P. Abbott and K. S. Ryder, *Chem. Rev.*, 2014, **114**, 11060–11082.
- Y. Pan, K. Sun, S. Liu, X. Cao, K. Wu, W.-C. Cheong, Z. Chen, Y. Wang, Y. Li, Y. Liu, D. Wang, Q. Peng, C. Chen and Y. Li, *J. Am. Chem. Soc.*, 2018, **140**, 2610–2618.
- H. Chen, K. Shen, Q. Mao, J. Chen and Y. Li, *ACS Catal.*, 2018, **8**, 1417–1426.
- A. Zhou, R.-M. Guo, J. Zhou, Y. Dou, Y. Chen and J.-R. Li, *ACS Sustainable Chem. Eng.*, 2018, **6**, 2103–2111.
- X. Liu, L. Xu, G. Xu, W. Jia, Y. Ma and Y. Zhang, *ACS Catal.*, 2016, **6**, 7611–7620.
- X. Yang, S. Wu, J. Hu, X. Fu, L. Peng, Q. Kan, Q. Huo and J. Guan, *Catal. Commun.*, 2016, **87**, 90–93.
- R. Nie, J. Shi, W. Du, W. Ning, Z. Hou and F.-S. Xiao, *J. Mater. Chem. A*, 2013, **1**, 9037.
- D. Wang, G. Yang, Q. Ma, M. Wu, Y. Tan, Y. Yoneyama and N. Tsubaki, *ACS Catal.*, 2012, **2**, 1958–1966.
- K. N. Kudin, B. Ozbas, H. C. Schniepp, R. K. Prud'homme, I. A. Aksay and R. Car, *Nano Lett.*, 2008, **1**, 36–41.
- K. M. Nam, J. H. Shim, H. Ki, S. I. Choi, G. Lee, J. K. Jang, Y. Jo, M. H. Jung, H. Song and J. T. Park, *Angew. Chem., Int. Ed.*, 2008, **47**, 9504–9508.
- P. Zhou, J. Liang, F. Wang, K. Deng, K. Lv and Z. Zhang, *Sci. Adv.*, 2017, **3**, e1601945.
- F. Jaouen, J. Herranz, M. Lefevre, J. P. Dodelet, U. I. Kramm, I. Herrmann, P. Bogdanoff, J. Maruyama, T. Nagaoka, A. Garsuch, J. R. Dahn, T. Olson, S. Pylypenko, P. Atanassov and E. A. Ustinov, *ACS Appl. Mater. Interfaces*, 2009, **1**, 1623–1639.
- J. Xiao, C. Chen, J. Xi, Y. Xu, F. Xiao, S. Wang and S. Yang, *Nanoscale*, 2015, **7**, 7056–7064.
- J. Long, B. Yin, Y. Li and L. Zhang, *AIChE J.*, 2014, **60**, 3565–3576.
- J. Long, K. Shen and Y. Li, *ACS Catal.*, 2016, **7**, 275–284.
- Z. Dong, Y. Li, J. Chen, B. Li, Y. Xing and J. Gao, *Org. Lett.*, 2005, **6**, 1043–1045.
- R. Noyori, M. Yamakawa and S. Hashiguchi, *J. Org. Chem.*, 2001, **24**, 7933.
- R. Noyori and S. Hashiguchi, *Acc. Chem. Res.*, 1997, **30**, 97–102.

- 37 J. Long, X. Xie, J. Xu, Q. Gu, L. Chen and X. Wang, *ACS Catal.*, 2012, **2**, 622–631.
- 38 J. C. Dupin, D. Gonbeau, P. Vinatier and A. Leasseur, *Phys. Chem. Chem. Phys.*, 2000, **2**, 1319–1324.
- 39 C. N. R. Rao, P. V. Kamath and S. Yashonath, *Chem. Phys. Lett.*, 1982, **88**, 13–16.
- 40 X. Bao, J. Deng and S. Dong, *Surf. Sci.*, 1985, **163**, 444–456.
- 41 R. L. Arechederra, K. Artyushkova, P. Atanassov and S. D. Minteer, *ACS Appl. Mater. Interfaces*, 2010, **2**, 3295–3302.
- 42 A. Morozan, P. Jegou, B. Jousselme and S. Palacin, *Phys. Chem. Chem. Phys.*, 2011, **13**, 21600–21607.
- 43 L. Zhang, A. Wang, W. Wang, Y. Huang, X. Liu, S. Miao, J. Liu and T. Zhang, *ACS Catal.*, 2015, **5**, 6563–6572.
- 44 M. C. Biesinger, B. P. Payne, A. P. Grosvenor, L. W. M. Lau, A. R. Gerson and R. S. C. Smart, *Appl. Surf. Sci.*, 2011, **257**, 2717–2730.
- 45 G. H. Jaffari, H.-Y. Lin, C. Ni and S. Ismat Shah, *Mater. Sci. Eng., B*, 2009, **164**, 23–29.